Microbial metabolite butyrate-prodrug polymeric micelles promote gut health and treat food allergies

Ruyi Wang[1,2*], Shijie Cao[1*], Mohamed Elfatih H. Bashir[1*], Lauren A. Hesser[1], Yanlin Su[3,4], Sung Min Choi Hong[3,4], Andrew Thompson[3,4], Elliot Culleen[3,4], Matthew Sabados[3], Nicholas P. Dylla[5], Evelyn Campbell[3,12], Altayeb A. Alshaikh[3,4], Ha-Na Shim[1], Hao Wu[1], Riyue Bao[6,7,8], D. Scott Wilson[1,9], Cathryn R. Nagler[1, 3,4,10+], Jeffrey A. Hubbell[1,10, 11+]

[*]These authors contributed equally to this work

[1]Pritzker School of Molecular Engineering, University of Chicago, Chicago, IL 60637, United States

[2]Department of Chemistry, University of Chicago, Chicago, IL 60637, United States

[3]Biological Sciences Division, University of Chicago, Chicago, IL 60637, United States

[4]Department of Pathology, University of Chicago, Chicago, IL 60637, United States

[5]Duchossois Family Institute, University of Chicago, Chicago, IL 60637, United States

[6]Department of Pediatrics, University of Chicago, Chicago, IL 60637, United States

[7]UPMC Hillman Cancer Center, Pittsburgh, PA 15232, United States

[8]Department of Medicine, University of Pittsburgh, Pittsburgh, PA 15232, United States

[9]Department of Biomedical Engineering, Johns Hopkins School of Medicine; Baltimore, MD 21231, United States

[10]Committee on Immunology, University of Chicago, Chicago, IL 60637, United States

[11]Committee on Cancer Biology, University of Chicago, Chicago, IL 60637, United States

[12]Committee on Microbiology, University of Chicago, Chicago, IL 60637, United States

[+]Co-senior authors to whom correspondence should be addressed:

cnagler1@uchicago.edu, jhubbell@uchicago.edu

Abstract

The gut microbiome modulates the body's response to food antigens[1]. Beneficial taxa, specifically butyrate-producing Clostridia, are depleted in food-allergic individuals[2,3]. Although butyrate is known to play important roles in regulating gut immunity and maintaining epithelial barrier function[4-6], its clinical translation is challenging due to its offensive odor and quick absorption in the upper gut. Here, we developed two polymeric micelle systems, one with a neutral charge (NtL-ButM) and one with a negative charge (Neg-ButM), that release butyrate from their polymeric core in the ileum or the cecum, respectively. Treatment with NtL-ButM in germ-free (and thus butyrate-depleted) mice up-regulated genes expressing antimicrobial peptides in the ileal epithelium. We show that these butyrate-containing micelles, used in combination, restore a barrier-protective response in mice treated with either dextran sodium sulfate or antibiotics. Treatment with the micelles protects peanut-allergic mice from an anaphylactic reaction to peanut challenge and rescues their dysbiosis by increasing the abundance of *Clostridium* Cluster XIVa. By restoring microbial and mucosal homeostasis, these butyrate-prodrug polymeric micelles may function as a new, antigen-agnostic approach to the treatment of food allergy.

Introduction

Food allergy is a prevalent and severe condition that affects over 32 million Americans[7]. Among adults with food allergy in the US, 38% reported at least one emergency department visit related to food allergy in their lifetime[7]. Recently, Palforzia was approved by the US FDA as an oral immunotherapy (OIT) for peanut allergy, becoming the first approved therapeutic for a food allergy[7]. The goal of the therapy is to establish a desensitized state by exposing patients to gradually increasing doses of peanut protein. Although OIT shows efficacy in inducing desensitization to peanut antigen, it requires a prolonged period of up-dosing, during which gastrointestinal symptoms are common[7]. Moreover, OIT is unlikely to achieve long-lasting non-responsiveness to peanut antigen in its current form[8]. Due to the adverse effects and limited efficacy of OIT, there is an urgent need to develop new therapies for food allergies.

The gut microbiome has many effects on both mucosal and systemic health[9]. Resident commensal bacteria play a critical role in the maintenance of mucosal homeostasis, in part through their production of short-chain fatty acids, especially butyrate[10-12]. Butyrate is produced by a subset of intestinal bacteria through the fermentation of dietary fiber[13]. Butyrate is the preferred energy substrate for colonic epithelial cells and strengthens gut barrier function by stabilizing hypoxia-inducible factor and maintaining epithelial tight junctions[12,14]. Butyrate also promotes the production of antimicrobial peptides (AMPs), which regulate intestinal homeostasis by shaping the composition of the microbiome[15]. To mediate its immunomodulatory functions butyrate acts via signaling through specific G protein coupled receptors or as an inhibitor of histone deacetylase activity (HDACs)[5]. HDAC inhibition by SCFAs promotes the differentiation of colonic regulatory T cells (Tregs)[16-18].

We have shown that neonatal administration of antibiotics reduces intestinal microbial diversity and impairs epithelial barrier function, resulting in increased access of food allergens to the

systemic circulation[19]. Administration of a consortium of spore-forming bacteria in the Clostridia class restored the integrity of the epithelial barrier and prevented allergic sensitization to food[19]. We went on to demonstrate a causal role for bacteria present in the healthy infant microbiota in protection against cow's milk allergy[3]. Transfer of the microbiota from healthy, but not cow's milk allergic (CMA), human infants into germ free (GF) mice protected against an anaphylactic response to a cow's milk allergen. By integrating differences in the microbiome signatures present in the healthy and CMA microbiotas with the changes each induced in ileal gene expression upon colonization of GF mice, we identified a single butyrate producing Clostridial species, *Anaerostipes caccae*, that mimicked the effects of the healthy microbiota upon monocolonization of GF mice[3]. Recent findings from a diverse cohort of twin children and adults concordant and discordant for food allergy validated the mouse model data with human microbiome samples. We found that most of the operational taxonomic units (OTUs) differentially abundant between healthy and allergic twins were in the Clostridia class; the broad age range of the twins studied indicated that an early-life depletion of allergy-protective Clostridia is maintained throughout life[2]. There is substantial interest in the use of butyrate-producing Clostridia as live biotherapeutics, but long-term engraftment of oxygen-sensitive anaerobic bacteria has proven challenging[20,21]. We therefore sought to explore butyrate itself as a candidate drug to maintain both microbial and mucosal homeostasis in the gut and to prevent or treat inappropriate allergic responses to food antigens.

Oral delivery of butyrate to the small intestine (where food antigens are absorbed) and large intestine (where most commensal bacteria reside) has been a challenge. Butyrate, even with enteric coating or encapsulation, possesses a foul and lasting odor and taste. As a sodium salt, orally administered butyrate is not absorbed in the part of the gut where it can have a therapeutic effect and is metabolized too rapidly to maintain a pharmacologic effect[22]. Previous work in murine models that demonstrated therapeutic effects of butyrate relied on high concentration, *ad libitum*

exposure to butyrate (mM quantities in drinking water) or utilized butyrylated starches[16-18,23-25]. A more controlled and practical delivery strategy is needed to exploit the potential therapeutic benefits of butyrate clinically to treat allergic and inflammatory diseases of the lower gastrointestinal (GI) tract.

To deliver butyrate throughout the GI tract, we designed block copolymers that can form water-suspendible micelles carrying a high content of butyrate in their core. These polymer formulations mask the smell and taste of butyrate and act as carriers to release the active ingredient (butyrate) over time as the micelles transit the GI tract. We show that these butyrate-conjugated polymer formulations up-regulate AMP gene expression in the ileal epithelium and modulate barrier integrity in antibiotic-treated mice and in mice treated with dextran sodium sulfate (DSS), a chemical perturbant that induces epithelial barrier dysfunction. Intragastric administration of our butyrate-prodrug micelles ameliorates an anaphylactic response to peanut challenge in a mouse model of peanut allergy and increases the abundance of bacteria in a cluster (*Clostridium* Cluster XIVa) known to contain butyrate-producing taxa. These findings pave the way for future clinical translation of butyrate micelles in treating food allergies.

Results

Co-polymers formulate butyrate into water-suspensible micelles

The block copolymer amphiphile pHPMA-b-pBMA was synthesized through two steps of reversible addition-fragmentation chain-transfer (RAFT) polymerization (**Fig. 1a**). The hydrophilic block was formed from N-(2-hydroxypropyl) methacrylamide (HPMA), while the hydrophobic block was from N-(2-butanoyloxyethyl) methacrylamide (BMA), thus connecting a backbone sidechain to butyrate with an ester bond. This ester bond can be hydrolyzed in the presence of esterase and releases butyrate in the GI tract, resulting in a water-soluble polymer as a final product. In addition to pHPMA-b-pBMA, we also synthesized pMAA-b-pBMA, which has an anionic

hydrophilic block formed from methacrylic acid (MAA) (**Fig. 1a**). At the block size ratios used herein, both pHPMA-b-pBMA and pMAA-b-pBMA contain 28% of butyrate by weight.

These block copolymers can be then formulated into nanoscale micelles to achieve high suspensibility in aqueous solutions as well as controlled release of butyrate from the core. The pHPMA-b-pBMA was self-assembled into neutral micelles (NtL-ButM) through a cosolvent evaporation method **(Fig. 1b**). The hydrophobic pBMA block forms the core, while the hydrophilic pHPMA forms the corona. In contrast, pMAA-b-pBMA cannot be formulated into micelles by this method because of the formation of intramolecular hydrogen bonds between pMAA chains[26]. Such bonding can, however, be disrupted when a strong base, here NaOH, is titrated into the mixture of pMAA-b-pBMA polymer to change methacrylic acid into ionized methacrylate[27-29]. Upon base titration, pMAA-b-pBMA polymer can then self-assemble into negatively charged micelles (Neg-ButM) (**Fig. 1b**). Cryogenic electron microscopy (CryoEM) revealed the detailed structure of the micelles, especially the core structure made of pBMA, which was more condensed with higher contrast. CryoEM images indicated that the diameter of the core of NtL-ButM was 30 nm, while Neg-ButM had a smaller core diameter of 15 nm (**Fig. 1c, d**). Both NtL-ButM and Neg-ButM have similar sizes of 44.7 ± 0.8 nm and 39.9 ± 1.6 nm, respectively, measured by dynamic light scattering (DLS) (**Fig. 1e**, **Fig. S10a**). Their low polydispersity index below 0.1 indicated the monodispersity of those micelles. As expected, NtL-ButM has a near-zero ζ-potential of -0.3 ± 0.5 mV, while Neg-ButM's is -31.5 ± 2.3 mV due to the ionization of methacrylic acid (**Fig. 1e**).To obtain the critical micelle concentration (CMC) of NtL-ButM and Neg-ButM, which indicates the likelihood of formation and dissociation of micelles in aqueous solutions, pyrene was added during the formulation and the fluorescence intensity ratio between the first and third vibronic bands of pyrene was plotted to calculate the CMC (**Fig. S11**)[30]. Results showed that Neg-ButM had a higher CMC of 14.0 ± 3.5 μM, compared to the CMC of NtL-ButM, which was 0.8 ± 0.3 μM (**Fig. 1e**). The higher CMC indicated that Neg-ButM micelles would be easier to dissociate in solution,

possibly because the surface charge made the micellar structure less stable compared to the neutral micelle NtL-ButM. In addition, we conducted small angle X-ray scattering (SAXS) analysis on both micelles to obtain the aggregation number (**Fig. S12**). As indicated from Guinier plots, radii of gyration for NtL-ButM and Neg-ButM were 14.2 nm and 13.5 nm (**Fig. 1e**), respectively, and the structures of micelles were confirmed to be spheres from Kratky plots of SAXS data (**Fig. S12**). We then fitted the SAXS data with a polydispersity core-shell sphere model with the assumptions that the micelle has a spherical core with a higher scattering length densities (SLD) and a shell with a lower SLD[31]. The model gave us the volume fraction of the micelles, the radius of the core, and the thickness of the shell, allowing us to calculate the aggregation number and mean distance between micelles. According to the fitting results, aggregation numbers for NtL-ButM and Neg-ButM were 119 and 92, respectively (**Fig. 1e**).

Butyrate micelles release butyrate in the lower GI tract

Given that butyrate is linked to the micelle-forming chain via ester bonds, we validated the release of butyrate in ex vivo conditions, including in simulated gastric fluid and simulated intestinal fluid that mimic those biological environments. In the simulated gastric fluid, both Neg-ButM and NtL-ButM showed negligible release of butyrate within hours, and sustained slow release over 3 weeks, while Neg-ButM had even slower release rate than NtL-ButM (**Fig. 2a**). The anionic surface of Neg-ButM in the acidic environment is likely responsible for the resistance to the hydrolysis of the BMA core. By contrast, in simulated intestinal fluid, both micelles released the most of their butyrate within minutes in the presence of a high concentration of the esterase pancreatin (**Fig. 2b**).

We then measured butyrate levels in the mouse GI tract after administering a single dose of NtL-ButM or Neg-ButM by intragastric gavage (i.g.). Both LC-UV and LC-MS/MS methods have been used to measure butyrate concentrations in the luminal contents of the ileum, cecum, and colon,

the sites where butyrate producing bacteria normally reside[32,33]. However, because the baseline concentration in the ileum was too low for the UV detector, we used LC-MS/MS to measure the butyrate concentration in that GI tract segment. NtL-ButM dramatically increased the butyrate concentration in the ileum for up to 2 hr after gavage (**Fig. 2c**), but this was short lived, and the butyrate concentration did not increase in either the cecum or colon **(Fig. 2d, e**). Interestingly, Neg-ButM raised butyrate concentrations by 3-fold in the cecum starting from 4 hr after gavage and lasting for at least another 8 hr but not in the ileum or colon (**Fig. 2c-e**). It is possible that the butyrate released in the cecum will continuously flow into the colon; our inability to detect increased concentrations of butyrate in the colon is likely due to its rapid absorption and metabolism by the colonic epithelium. In addition, as expected the polymer backbone of the micelles remained intact when passing through the GI tract. We observed less than 28% molecular weight loss – the percentage of butyrate content – of the polymer in fecal samples collected from 4–8 hr after oral administration (**Fig. S14 a, b**). Moreover, when incubated in a hydrolytic environment in vitro, the polymer backbone remained intact after releasing most of the butyrate over 7 days in 125 mM sodium hydroxide solution (**Fig. S14 c, d**).

We further investigated how these two butyrate micelles transit through the GI tract by administering fluorescently labeled NtL-ButM or Neg-ButM to mice i.g. and visualizing their biodistribution via an In Vivo Imaging System (IVIS) (**Fig. S15**). In this case, the fluorescent marker was conjugated to the polymer chain, allowing visualization of the transit of the polymer backbone itself. The IVIS results validated that the polymeric micelles were retained in the mouse GI tract for more than 6 hr. after gavage. The neutral micelle NtL-ButM passed through the stomach and small intestine within 2 hr. and accumulated in the cecum. However, negatively charged Neg-ButM accumulated in the stomach first and then gradually traveled through the small intestine to the cecum. Overall, Neg-ButM had a longer retention time in the stomach and small intestine, which is possibly due to the stronger adhesive effect to the gut mucosa[26,34,35]. Both

micelles were cleared from the GI tract within 24 hr. after administration. In addition, we measured the fluorescence signal from other major organs and plasma by IVIS (**Fig. S15b**), as well as the butyrate concentration in the plasma by LC-MS/MS. The signals were all below the detection limit from both methods, suggesting that there was negligible absorption of these butyrate micelles into the blood circulation from the intestine, consistent with our desire to deliver butyrate to the lower GI tract and to avoid any complexities of systemic absorption of the polymer or micelles.

Ileum-targeting butyrate micelles up-regulate AMP genes in the ileal epithelium

Delivery of butyrate to the lower GI tract could affect the host immune response by interacting with the intestinal epithelium. To investigate whether and how our butyrate micelles regulate gene expression in the distal small intestine, we performed RNA sequencing of the ileal epithelial cell compartment (**Fig. 3a**). Germ-free (and thus butyrate-depleted) C3H/HeN mice were treated daily with NtL-ButM i.g. for one week and ileal epithelial cells were collected for RNA isolation and sequencing. Because only NtL-ButM (and not Neg-ButM) released butyrate in the ileum, only NtL-ButM was used for this experiment to examine local effects. NtL-ButM-treated mice had unique gene expression signatures compared to those treated with PBS or control polymer, which consists of the same polymeric structure but does not contain butyrate. Such differences showed no dependence on sex. Interestingly, most genes upregulated by NtL-ButM treatment were Paneth cell derived antimicrobial peptides (AMPs), including angiogenin 4 (Ang4), lysozyme-1 (Lyz1), intelectin (Itln1) and several defensins (Defa3, Defa22, Defa24 etc.) (**Fig. 3a, Fig. S16**). We quantified the protein level of intelectin, one of the up-regulated AMPs (**Fig. 3b, c**). We chose intelectin because it is known to be expressed by Paneth cells which reside in small intestinal crypts and can recognize the carbohydrate chains of the bacterial cell wall[36]. Paneth cell AMPs have largely been characterized in C57BL/6 mice and specific reagents are available for their detection in that strain[37]. GF C57BL/6 mice were gavaged daily with NtL-ButM or PBS for one week. Immunofluorescence microscopy of ileal sections revealed that the NtL-ButM treated group

expressed a large amount of intelectin in the crypts of the ileal tissue. However, images from the PBS group showed limited intelectin signal (**Fig. 3b**). Quantification using ImageJ of relative fluorescence intensity per ileal crypt also showed that the NtL-ButM group had significantly higher expression of intelectin compared to the PBS control (**Fig. 3c**). The intelectin staining thus further supported the pharmacological effects of NtL-ButM; up-regulation of intelectin induced by NtL-ButM was not only demonstrated on the transcriptional level by RNAseq but was also validated at the protein level.

Butyrate micelles repair intestinal barrier function

As discussed above, butyrate-producing bacteria play an important role in the maintenance of the intestinal barrier. To assess the effects of locally-delivered butyrate on intestinal barrier integrity, we treated mice with the chemical perturbant DSS for 7 days to induce epithelial barrier dysfunction[38]. Due to the different biodistribution and butyrate release behaviors in vivo from the two butyrate micelles, we reasoned that the combined dosing of NtL-ButM and Neg-ButM would cover the longest section of the lower GI tract and last for a longer time; thus, a 1:1 combination of NtL-ButM and Neg-ButM (abbreviated as ButM) was selected for study. Throughout DSS treatment, and for three days after DSS administration was terminated, mice were orally gavaged twice daily with either PBS or ButM at three different concentrations, or once daily with cyclosporin A (CsA) as the positive therapeutic control (as outlined in **Fig. 4a**). Intragastric gavage of 4 kDa FITC-dextran was used to evaluate intestinal barrier permeability. We detected a significantly higher concentration of FITC-dextran in the serum of DSS-treated mice gavaged only with PBS, demonstrating an impaired intestinal barrier. Naïve mice (without DSS exposure), or the DSS-treated mice that also received either CsA or ButM at all three concentrations had similar serum levels of FITC-dextran, suggesting that treatment with ButM successfully repaired the DSS-induced injury to the barrier (**Fig. 4b**). Additionally, neonatal antibiotic treatment impairs homeostatic epithelial barrier function and increases permeability to food antigens[19]. Thus, we

further evaluated whether the ButM treatment can reduce intestinal barrier permeability in antibiotic-treated mice (**Fig. 4c**). Similar to what we observed in the DSS-induced model, the mice treated with ButM had significantly lower FITC-dextran levels in the serum compared to mice that received PBS (**Fig. 4d**), demonstrating that ButM effectively rescued both DSS-induced and antibiotic-induced intestinal barrier dysfunction.

Butyrate micelles ameliorated anaphylactic responses in peanut allergic mice

To evaluate the efficacy of the butyrate-containing micelles in treating food allergy, we tested ButM in a well-established murine model of peanut-induced anaphylaxis[19,39]. All of the mice were treated with vancomycin to induce dysbiosis. Beginning at weaning, vancomycin-treated SPF C3H/HeN mice were intragastrically sensitized weekly for 4 weeks with peanut extract (PN) plus the mucosal adjuvant cholera toxin (CT) (**Fig. 5a, b**), as previously described[19,39]. Following sensitization, some of the mice were challenged with intraperitoneal (i.p.) PN and their change in core body temperature was monitored to ensure that the mice were uniformly sensitized; a decrease in core body temperature is indicative of anaphylaxis (**Fig. 5c**). The rest of the sensitized mice were then treated i.g. twice daily for 2 weeks with either PBS or the combined micelle formulation ButM. After 2 weeks of therapy, the mice were challenged by i.p. injection of PN and their core body temperature was assessed to evaluate the response to allergen challenge. Compared with PBS-treated mice, allergic mice that were treated with ButM experienced a significantly reduced anaphylactic drop in core body temperature (**Fig. 5d**). In addition, ButM-treated mice also had significantly reduced concentrations of mouse mast cell protease-1 (mMCPT-1) and peanut-specific IgE detected in the serum (**Fig. 5e, f**). mMCPT-1 is a chmyase expressed by intestinal mucosal mast cells; elevated concentrations of mMCPT-1 increase intestinal barrier permeability during allergic hypersensitivity responses[40,41]. Furthermore, these effects of ButM on the peanut allergic mice were dose-dependent, as we observed that reducing the dose of ButM by half was not as effective as the full dose in protecting mice from an

anaphylactic response (**Fig. S17**). Together, these results demonstrate that ButM as a monotherapy can effectively prevent allergic responses to food in sensitized mice.

Because OIT is the only FDA-approved treatment for peanut allergy, we also tested whether ButM would be an effective treatment when delivered synchronously with low dose exposure to allergen in sensitized mice (**Fig. S18a, b**). We observed that low-dose PN treatment alone in this regimen had no therapeutic effect, possibly due to insufficient length of treatment to achieve functional OIT, as low-dose PN-treated mice had a comparable drop in core body temperature to those that received no treatment (**Fig. S18c, d**). However, mice treated with low-dose PN plus ButM exhibited a significantly reduced drop in core body temperature indicative of a substantially decreased anaphylactic response. This suggests a potential clinical use of butyrate micelles for patients undergoing OIT. However, the treatment did not reduce serum peanut-specific IgE, as has been observed in several clinical studies of OIT[8,42] (**Fig. S18f**).

Butyrate micelles alter fecal microbiota and promote recovery of Clostridia after antibiotic exposure

Given that ButM induces AMPs and may alter gut metabolism, we examined whether treatment altered the fecal microbiome. In the mouse model of peanut allergy described above, we induced dysbiosis by treating mice with vancomycin one week before the start of allergen sensitization and throughout the sensitization regimen. Vancomycin depletes Gram positive bacteria, including Clostridial species[43]. After sensitization, we removed vancomycin from the drinking water and compared the fecal microbial composition of the allergic mice before and after treatment with PBS or ButM (see timepoints collected in **Fig. 5a**). 16S rRNA targeted sequencing confirmed depletion of Clostridia in vancomycin-treated mice; the fecal microbiota was instead dominated by Lactobacillus and Proteobacteria (**Fig. 6a**, left). After halting vancomycin administration, regrowth of Clostridia (including Lachnospiraceae and others) and Bacteroidetes was observed in both the

PBS and ButM treated groups (**Fig. 6a**, right, **Fig. S19**). When comparing differentially abundant taxa between treatment groups by LEfSe analysis, *Murimonas* and *Streptococcus* were significantly higher in relative abundance in the PBS post-treatment group when compared to the ButM post-treatment group (**Fig. 6b**). ButM treatment significantly increased the relative abundance of *Enterococcus*, *Coprobacter*, and *Clostridium* Cluster XIVa (**Fig. 6b**). *Clostridium* Cluster XIVa is a numerically predominant group of bacteria (in both mice and humans) that is known to produce butyrate, modulate host immunity, and induce Tregs[43,44]. We confirmed that the relative abundance of *Clostridium* Cluster XIVa in mice treated with ButM was significantly increased in the 16S data set (**Fig. 6c**) and quantified the enriched abundance of this taxa by qPCR (**Fig. 6d)**. Our finding of increased abundance of *Clostridium* Cluster XIVA after treatment with ButM is in keeping with earlier work which showed that butyrate sensing by peroxisome proliferator-activated receptor (PPAR-γ) shunts colonocyte metabolism toward β-oxidation, creating a local hypoxic niche for these oxygen sensitive anaerobes[45].

We also carried out initial characterization of toxicity of the butyrate micelles. Specifically, we demonstrated that treatment induced no changes among the serological toxicity markers tested, including serum albumin, alanine aminotransferase, amylase, blood urea nitrogen, calcium, and total protein, over a 6-week course of daily treatment (**Fig. S20**). These findings pave the way for the future clinical translation of butyrate micelles in treating food allergies.

Discussion

The prevalence of food allergy has increased dramatically over the past 20 years, particularly in developed countries[7,46]. Lifestyle changes such as reduced consumption of dietary fiber, increased antibiotic use (including in the food chain), and sanitation, have altered populations of commensal microbes. These alterations lead to several negative health effects, including impairment of intestinal barrier function. Modulating the gut microbiome to redirect immunity has

become a substantial effort in both academia and industry. However, this has proven difficult: getting selected organisms, especially obligate anaerobes, to colonize the gut is far from straightforward. Here, we have instead focused on delivering the metabolites that are produced by these organisms in a more direct manner, as one of the main modes of action of these organisms is through their metabolites.

Specifically, we developed a polymeric nano-scale system to deliver butyrate to localized regions along the GI tract. The system was based on polymeric micelles formed by block copolymers, in which butyrate is conjugated to the hydrophobic block by an ester bond and can be hydrolyzed by esterases in the GI tract for local release. The linked butyrate moieties drive hydrophobicity in that block and, as release occurs, the remainder of the construct (an inert, water-soluble polymer) continues to transit through the lower GI tract until it is excreted. The butyrate-containing block, when forming the core of micelles, was resistant to the acidic environment found in the stomach, which might prevent a burst release there before the micelle's transit into the intestine. The two butyrate-prodrug micelles, NtL-ButM and Neg-ButM, share similar structures but have corona charges of neutral and negative, respectively. This results in their distinct biodistribution in the lower GI tract, where they can release butyrate in the presence of enzymes. Here, to treat a mouse model of peanut allergy and to repair intestinal barrier dysfunction, we combined both the neutral and negatively charged micelles to deliver butyrate along the distal gut and showed successful preservation of barrier function and protection from severe anaphylactic responses with a short-term treatment. Our butyrate micelles were not absorbed in the small intestine and could act locally by inducing a gene expression signature that is comprised almost entirely of AMPs. These AMPs, mainly expressed by specialized Paneth cells in the ileum, are essential for maintaining the balance of the ileal microbiome[15]. In our mouse model of peanut allergy, where the mice were previously exposed to vancomycin to induce dysbiosis, we showed that ButM treatment could favorably increase the relative abundance of protective bacteria, such as

Clostridium Cluster XIVa. Bacteria in *Clostridium* Cluster XIVa are known to induce local Tregs in preclinical models and may be critical to the success of fecal microbiota transplant for treatment of colitis [43,47]. Increasing the abundance of these bacteria may be one mechanism by which ButM treatment improves epithelial barrier function after exposure to DSS or antibiotics.

Investigations of the therapeutic potential of butyrate in animal models have supplemented butyrate in the drinking water or diet at a high dose for three or more weeks[16-18,23-25]. Such dosing to achieve therapeutic effects from sodium butyrate is challenging for clinical translation, due to the uncontrolled dosing regimen, difficulties to replicate in humans, and the unpleasant odor and taste of butyrate as a sodium salt. Our formulation has incorporated butyrate in the polymeric micelles at a high load (28 wt%) and is able to deliver and release most of the butyrate in the lower GI tract, in a manner that masks butyrate's taste and smell. Here, we have used a daily dose of 800 mg/kg of total ButM to treat peanut allergic mice for two weeks. This can be translated to ~65 mg/kg of total ButM (or equivalent butyrate dose of 18.2 mg/kg) human dose given the differences in body surface area between rodents and the human[48]. This butyrate dose in ButM micelles is comparable to other butyrate dosage forms that has been tested clinically[49-51], however, through the local targeting and sustained release in the lower GI tract, we expect our ButM formulation to achieve higher therapeutic potential in food allergies and beyond.

Our approach is not antigen-specific, since antigen delivery was not part of the main regimen: our initial proof-of-concept in peanut allergy could be readily extended to other food allergens, such as other nuts, milk, egg, soy and shellfish. Moreover, our platform can also be easily adapted to deliver other SCFAs or other microbiome-derived metabolites in a single form or in combination, providing a more controlled and accessible way to achieve potential therapeutic efficacy.

Materials and Methods

Materials for polymer synthesis

N-(2-hydroxyethyl) methacrylamide (HPMA) monomer was obtained from Sigma-Aldrich or Polysciences, Inc. Solvents including dichloromethane, methanol, hexanes, and ethanol were ACS reagent grade and were obtained from Fisher Scientific. All other chemicals were obtained from Sigma-Aldrich.

Synthesis of N-(2-hydroxyethyl) methacrylamide (2)

To synthesize N-(2-hydroxyethyl) methacrylamide (HEMA, **2**), ethanolamine (3.70 mL, 61.4 mmol, 2.0 eq), triethylamine (4.72 mL, 33.8 mmol, 1.1 eq) and 50 mL DCM were added into a 250 mL flask. After the system was cooled by an ice bath, and methacryloyl chloride (**1**, 3.00 mL, 30.7 mmol, 1.0 efq) was added dropwise under the protection of nitrogen. The reaction was allowed to warm to room temperature and reacted overnight. Then the reaction mixture was concentrated by rotary evaporation and purified on a silica column using DCM/MeOH (MeOH fraction v/v from 0% to 5%). The product was obtained as a colorless oil (3.42 g, 86.3%). MS (ESI). $C_6H_{11}NO_2$, m/z calculated for $[M+H]^+$: 129.08, found: 129.0. ^{1}H-NMR (500 MHz, $CDCl_3$) δ 1.93 (s, 3H), 3.43 (m, 2H), 3.71 (m, 2H), 5.32 (s, 1H), 5.70 (s, 1H), 6.44 (br s, 1H) (**Fig. S1**).

Synthesis of N-(2-butanoyloxyethyl) methacrylamide (3)

To synthesize N-(2-butanoyloxyethyl) methacrylamide (BMA, **3**), N-(2-hydroxyethyl) methacrylamide (3.30 mL, 25.6 mmol, 1.0 eq), triethylamine (7.15 mL, 51.2 mmol, 2.0 eq) and 50 mL DCM were added into a 250 mL flask. After the reaction system was cooled by an ice bath, butyric anhydride (5.00 mL, 30.7 mmol, 1.2 eq) was added dropwise under the protection of nitrogen. The system was allowed to react overnight. The reaction mixture was filtered and washed by NH_4Cl solution, $NaHCO_3$ solution, and water. After drying by anhydrous $MgSO_4$, the

organic layer was concentrated by rotary evaporation and purified on a silica column using DCM/MeOH (MeOH fraction v/v from 0% to 5%). The product was obtained as a pale-yellow oil (4.56 g, 89.6%). MS (ESI). $C_{10}H_{17}NO_3$, m/z calculated for $[M+H]^+$: 199.12, found: 199.1. ^{1}H-NMR (500 MHz, $CDCl_3$) δ 0.95 (t, 3H), 1.66 (m, 2H), 1.97 (s, 3H), 2.32 (t, 2H), 3.59 (dt, 2H), 4.23 (t, 2H), 5.35 (s, 1H), 5.71 (s, 1H), 6.19 (br s, 1H) (**Fig. S2**).

Synthesis of poly(2-hydroxypropyl methacrylamide) (pHPMA, 5)

pHPMA was prepared using 2-cyano-2-propyl benzodithioate as the RAFT chain transfer agent and 2,2'-Azobis(2-methylpropionitrile) (AIBN) as the initiator. Briefly, HPMA (**4**, 3.0 g, 20.9 mmol, 1.0 eq), 2-cyano-2-propyl benzodithioate (28.3 mg, 0.128 mmol, 1/164 eq), and AIBN (5.25 mg, 0.032 mmol, 1/656 eq) were dissolved in 10 mL MeOH in a 25 mL Schlenk tube. The reaction mixture was subjected to four freeze-pump-thaw cycles. The polymerization was conducted at 70°C for 30 hr. The polymer was precipitated in a large volume of petroleum ether and dried in the vacuum chamber overnight. The product obtained was a light pink solid (1.8 g, 60 %). ^{1}H-NMR (500 MHz, DMSO-d6) δ 0.8-1.2 (m, 6H, CH(OH)-CH_3 and backbone CH_3), 1.5-1.8 (m, 2H, backbone CH_2), 2.91 (m, 2H, NH-CH_2), 3.68 (m, 1H, C(OH)-H), 4.70 (m, 1H, CH-OH), 7.18 (m, 1H, NH) (**Fig. S3**).

Synthesis of pHPMA-b-pBMA (6)

The block copolymer pHPMA-b-pBMA was prepared using pHPMA (**5**) as the macro-RAFT chain transfer agent and N-(2-butanoyloxyethyl) methacrylamide (**3**) as the monomer of the second RAFT polymerization. Briefly, pHPMA (1.50 g, 0.105 mmol, 1.0 eq), N-(2-butanoyloxyethyl) methacrylamide (4.18 g, 21.0 mmol, 200 eq), and AIBN (8.3 mg, 0.050 mmol, 0.50 eq) were dissolved in 10 mL MeOH in a 50 mL Schlenk tube. The reaction mixture was subjected to four freeze-pump-thaw cycles. The polymerization was conducted at 70°C for 20 hr. The polymer was precipitated in petroleum ether and dried in the vacuum chamber overnight. The product obtained

was a light pink solid (4.22 g, 74%). ^{1}H-NMR (500 MHz, DMSO-d6) δ 0.80-1.1 (m, 9H, CH(OH)-CH_3 (HPMA), CH_2-CH_3 (BMA), and backbone CH_3), 1.55 (m, 4H, CH_2-CH_2 (BMA) and backbone CH_2), 2.28 (m, 2H, CO-CH_2 (BMA)), 2.91 (m, 2H, NH-CH_2 (HPMA)), 3.16 (m, 2H, NH-CH_2 (BMA)), 3.67 (m, 1H, CH(OH)-H), 3.98 (m, 2H, O-CH_2 (BMA)), 4.71 (m, 1H, CH-OH (HPMA)), 7.19 (m, 1H, NH), 7.44 (m, 1H, NH) (**Fig. S4**).

Synthesis of pMAA (7) and pMAA-b-pBMA (8)

pMAA (**7**) was prepared using 2-cyano-2-propyl benzodithioate as the RAFT chain transfer agent and AIBN as the initiator. Briefly, methacrylic acid (MAA) (4.0 mL, 47.2 mmol, 1.0 eq), 2-cyano-2-propyl benzodithioate (104.4 mg, 0.472 mmol, 1/100 eq), and AIBN (19.4 mg, 0.118 mmol, 1/400 eq) were dissolved in 20 mL MeOH in a 50 mL Schlenk tube. The reaction mixture was subjected to four freeze-pump-thaw cycles. The polymerization was conducted at 70°C for 24 hr. The polymer was precipitated in hexanes and dried in the vacuum oven overnight. The product obtained was a light pink solid (4.0 g, 100 %). ^{1}H-NMR (500 MHz, DMSO-d6) δ 0.8-1.2 (m, 3H, backbone CH_3), 1.5-1.8 (m, 2H, backbone CH_2), 7.4-7.8 (three peaks, 5H, aromatic H), 12.3 (m, 1H, CO-OH) (**Fig. S5**).

The block copolymer pMAA-b-pBMA (**8**) was prepared using (**7**) pMAA as the macro-RAFT chain transfer agent and (**3**) N-(2-butanoyloxyethyl) methacrylamide (BMA) as the monomer of the second RAFT polymerization. Briefly, pMAA (0.50 g, 0.058 mmol, 1.0 eq), N-(2-butanoyloxyethyl) methacrylamide (1.47 g, 7.38 mmol, 127 eq), and AIBN (2.4 mg, 0.015 mmol, 0.25 eq) were dissolved in 10 mL MeOH in a 25 mL Schlenk tube. The reaction mixture was subjected to four freeze-pump-thaw cycles. The polymerization was conducted at 70°C for 24 hr. The polymer was precipitated in hexanes and dried in the vacuum oven overnight. The product obtained was a light pink solid (1.5 g, 70%). ^{1}H-NMR (500 MHz, DMSO-d6) δ 0.8-1.1 (m, 6H, CH_2-CH_3 (BMA), and backbone CH_3), 1.5-1.7 (m, 4H, CH_2-CH_2 (BMA) and backbone CH_2), 2.3 (m, 2H, CO-CH_2 (BMA)),

3.2 (m, 2H, NH-CH_2 (BMA)), 4.0 (m, 2H, O-CH_2 (BMA)), 7.4 (m, 1H, NH), 12.3 (m, 1H, CO-OH) (**Fig. S6**).

Synthesis of N_3-PEG_4-MA (9) and azide-PEG polymer

In order to include an azide group into pHPMA-b-pBMA or pMAA-b-pBMA polymers, monomer N-(2-(2-(2-(2-azidoethoxy)ethoxy)ethoxy)ethyl) methacrylamide (**9**) was synthesized and used in the copolymerization with HPMA or MAA to obtain the hydrophilic block with azide function. Briefly, N_3-PEG_4-NH_2 (0.5 g, 2.14 mmol, 1.0 eq) and triethylamine (0.60 mL, 4.3 mmol, 2.0 eq) were dissolved in anhydrous DCM. After the reaction system was cooled by an ice bath, methacrylic chloride (0.42 mL, 2.6 mmol, 1.2 eq) was added dropwise under the protection of nitrogen. The system was allowed to react overnight. The reaction mixture was filtered and washed by NH_4Cl solution, $NaHCO_3$ solution, and water. After being dried by anhydrous $MgSO_4$, the organic layer was concentrated by rotary evaporation and purified on a silica column using DCM/MeOH (MeOH fraction v/v from 0% to 5%). The product obtained was a pale-yellow oil (0.47 g, 73 %). MS (ESI). $C_{12}H_{22}N_4O_4$, m/z calculated for $[M+H]^+$: 287.16, found: 287.2. ^{1}H-NMR (500 MHz, $CDCl_3$) δ 6.35 (br, 1H), 5.70 (s, 1H), 5.32 (s, 1H), 3.55-3.67 (m, 12H), 3.52 (m, 2H), 3.38 (t, 2H), 1.97 (s, 3H) (**Fig. S7**). Monomer N_3-PEG_4-MA was mixed with HPMA or MAA in a 2:98 wt:wt ratio during the RAFT polymerization to obtain N_3-pHPMA or N_3-pMAA. Then, the second block of BMA was added to the macro initiator to obtain N_3-pHPMA-b-pBMA or N_3-pMAA-b-pBMA, respectively. The synthesis procedures were the same as the previous description.

Synthesis of N-hexyl methacrylamide (10) and control polymer

In order to synthesize a control polymer that did not contain butyrate ester, monomer N-hexyl methacrylamide (**11**) was synthesized and used in the polymerization of hydrophobic block. Briefly, hexanamine (5.8 mL, 46.0 mmol, 1.5 eq), triethylamine (4.7 mL, 33.8 mmol, 1.1 eq) and

50 mL DCM were added into a 250 mL flask. After the system was cooled by an ice bath, methacryloyl chloride (3.0 mL, 30.7 mmol, 1.0 eq) was added dropwise under the protection of nitrogen. The reaction was allowed to warm to room temperature and reacted overnight. Then the reaction mixture was concentrated by rotary evaporation and purified on a silica column using DCM/MeOH (MeOH fraction v/v from 0% to 5%). The product obtained was a colorless oil (4.6 g, 88%). MS (ESI). $C_{11}H_{21}NO$, m/z calculated for $[M+H]^+$: 184.16, found: 184.2. ^{1}H-NMR (500 MHz, $CDCl_3$) δ 5.75 (br, 1H), 5.66 (s, 1H), 5.30 (s, 1H), 3.31 (t, 2H), 1.96 (s, 3H), 1.54 (m, 2H), 1.28-1.32 (m, 8H), 0.88 (t, 3H) (**Fig. S8**). After the synthesis of pHPMA or pMAA, monomer N-hexyl methacrylamide (**11**) was used in the polymerization of second block instead of N-(2-butanoyloxyethyl) methacrylamide to obtain control polymers as pHPMA-b-pHMA or pMAA-b-pHMA, respectively (**Fig. S9**). The synthesis procedures were the same as described above.

Formulation of polymeric micelles

NtL-ButM micelle was formulated by cosolvent evaporation method. 80 mg of pHPMA-b-pBMA polymer was dissolved in 10 mL of ethanol under stirring. After the polymer was completely dissolved, the same volume of 1 × PBS was added slowly to the solution. The solution was allowed to evaporate at room temperature for at least 6 hr until ethanol was removed. After the evaporation, the NtL-ButM solution was filtered through a 0.22 μm filter and stored at 4°C. The size of the micelles was measured by DLS.

Neg-ButM micelle was prepared by base titration[27,28]. 60 mg of pMAA-b-pBMA polymer was added to 8 mL of 1 × PBS under vigorous stirring. Sodium hydroxide solution in molar equivalent to methacrylic acid was added to the polymer solution in three portions over the course of 2 hr. After adding base solution, the polymer solution was stirred at room temperature overnight.1 × PBS was then added to reach the target volume and the solution was filtered through a 0.22 μm

filter. The pH of the solution was checked to confirm it was neutral, and the size of the micelles was measured by DLS.

Dynamic light scattering (DLS) characterizations of micelles

DLS data was obtained from a Zetasizer Nano ZS90 (Malvern Instruments). Samples were diluted 400 times in 1 × PBS and 700 µL was transferred to a DLS cuvette for data acquisition. The intensity distributions of DLS were used to determine the hydrodynamic diameter of micelles. For zeta-potential data, micelles were diluted 100 times in 0.1 × PBS (1:10 of 1 × PBS to MilliQ water) and transferred to disposable folded capillary zeta cells for data acquisition.

Cryogenic electron microscope imaging of micelles

CryoEM images were acquired on a FEI Talos 200kV FEG electron microscope. Polymeric nanoparticle samples were prepared in 1 × PBS and diluted to 2 mg/mL with MilliQ water. 2 µL sample solution was applied to electron microscopy grid (Agar Scientific) with holey carbon film. Sample grids were blotted, and flash vitrified in liquid ethane using an automatic plunge freezing apparatus (Vitrbot) to control humidity (100%) and temperature (20°C). Analysis was performed at -170°C using the Gatan 626 cry-specimen holder (120,000× magnification; -5 µm defocus). Digital images were recorded on an in-line Eagle CCD camera and processed by ImageJ.

Measurement of critical micelle concentration

The critical micelle concentrations of NtL-ButM and Neg-ButM were determined by a fluorescence spectroscopic method using pyrene as a hydrophobic fluorescent probe[30,52]. A series of polymer solutions with concentration ranging from 1.0×10^{-4} to 2.0 mg mL^{-1} were mixed with pyrene solution with a concentration of 1.2×10^{-3} mg mL^{-1}. The emission spectra of samples were recorded on a fluorescence spectrophotometer (HORIBA Fluorolog-3) at 20°C using 335 nm as excitation wavelength. The ratio between the first (372 nm) and the third (383 nm) vibronic band

of pyrene was used to plot against the concentration of the polymer. The data were processed on Prism software and fitted using Sigmoidal model (**Fig. S11**).

Small angle x-ray scattering analysis of micelles

SAXS samples were made in 1 × PBS and filtered through 0.2 μm filters. All samples were acquired at Stanford Synchrotron Radiation Lightsource, SLAC National Accelerator Laboratory. SAXS data were analyzed by Igor Pro 8 software (**Fig. S12**). To acquire radius of gyration (R_g), data were plotted as ln(intensity) vs. q^2 at low q range. Then R_g were calculated from the slope of the linear fitting as shown in the equation (1).

$$ln(I(q)) = ln(I(0)) - \frac{q^2 R_g^2}{3} \quad (1)$$

Kratky plot of the data were plotted from I q^2 vs. q to show the structure of the particles. Moreover, the data were fitted using polydispersed core-shell sphere model (**Fig. S12f,g**)[31]. From the fitting, the radius of the core, thickness of the shell, and volume fraction of the micelle were derived and used to calculate the molecular weight of micelle and the mean distance between micelles using flowing equations:

$$N = \frac{\phi_{micelle}}{v_{micelle}} \quad (2)$$

$$M_w = \frac{cN_A}{N} \quad (3)$$

$$d = N^{-1/3} \times 10^7 \quad (4)$$

where N is the number of micelles per unit volume. $\phi_{micelle}$ is the volume fraction of micelles derived from fitting. $v_{micelle}$ is the volume of a single micelle, which is calculated from 4/3 πR^3, where R is

the sum of radius of core and thickness of shell. M_w is the molecular weight of micelle. c is the polymer concentration. N_A is Avogadro constant. d is the mean distance between the micelles in the unit of nm. The aggregation number of micelles were calculated from dividing the molecular weight of micelle by the molecular weight of polymer.

Mice

C3H/HeN and C3H/HeJ mice were maintained in a Helicobacter, Pasteurella and murine norovirus free, specific pathogen-free (SPF) facility at the University of Chicago. Breeding pairs of C3H/HeJ mice were originally purchased from the Jackson Laboratory. Breeding pairs of C3H/HeN mice were transferred from the germ-free (GF) facility. All experimental mice were bred in house and weaned at 3 weeks of age onto a plant-based mouse chow (Purina Lab Diet 5K67®) and autoclaved sterile water. Mice were maintained on a 12 h light/dark cycle at a room temperature of 20–24 °C. GF C3H/HeN or C57BL/6 mice were bred and housed in the Gnotobiotic Research Animal Facility (GRAF) at the University of Chicago. GF mice were maintained in Trexler-style flexible film isolator housing units (Class Biologically Clean) with Ancare polycarbonate mouse cages (catalog number N10HT) and Teklad Pine Shavings (7088; sterilized by autoclave) on a 12 h light/dark cycle at a room temperature of 20–24 °C. All experiments were littermate controlled. All protocols used in this study were approved by the Institutional Animal Care and Use Committee of the University of Chicago. The FITC-dextran intestinal permeability assay in DSS treated mice was performed by Inotiv (Boulder, CO); SPF C57BL/6 mice were obtained from Taconic and housed in the Inotiv animal facility. The study was conducted in accordance with *The Guide for the Care & Use of Laboratory Animals (8th Edition)* and therefore in accordance with all Inotiv IACUC approved policies and procedures.

Biodistribution study using in vivo imaging system (IVIS)

SPF C3H/HeJ mice were used for biodistribution studies. Azide labeled pHPMA-b-pBMA or pMAA-b-pBMA polymer was reacted with IR 750-DBCO (Thermo Fisher) and purified by hexane precipitation. After formulation into micelles, the fluorescently labeled NtL-ButM, or Neg-ButM was administered to mice by i.g. gavage. After 1 hr, 3 hr, 6 hr, or 24 hr, mice were euthanized, the major organs were collected from the mice and whole-organ fluorescence was measured via an IVIS Spectrum in vivo imaging system (Perkin Elmer). Images were processed and analyzed by Living Imaging 4.5.5 (Perkin Elmer).

Butyrate derivatization and quantification using LC-UV or LC-MS/MS

Simulated gastric fluid and simulated intestinal fluid (Fisher Scientific) were used for in vitro release analysis as described previously[53,54]. NtL-ButM or Neg-ButM were added to simulated gastric fluid or simulated intestinal fluid at a final concentration of 2 mg/mL at 37°C. At pre-determined time points, 20 µL of the solution was transferred into 500 µL of water:acetonitrile 1:1 v/v. The sample was centrifuged using Amicon Ultra filters (Merck, 3 kDa molecular mass cutoff) at 13,000 × g for 15 min to remove polymers. The filtrate was stored at -80°C before derivatization. For the in vivo release study in mouse GI tract, NtL-ButM or Neg-ButM micelle solutions were i.g. administered to SPF C3H/HeJ mice at 0.8 mg per g of body weight. Mice were euthanized at 1 hr, 2 hr, 4 hr, 8 hr, 12 hr, and 24 hr after the gavage. Luminal contents from the ileum, cecum, or colon were collected in an EP tube. After adding 500 µL of 1 × PBS, the mixture was vortexed and sonicated for 10 min, and then centrifuged at 13,000 × g for 10 min. The supernatant was transferred and filtered through 0.45 m filter. The filtered solution was stored at -80°C before derivatization.

Sample derivatization (**Fig. S13a**): Samples were prepared and derivatized as described in the literature[32]. 3-nitrophenylhydrazine (NPH) stock solution was prepared at 0.02 M in water:acetonitrile 1:1 v/v. EDC stock solution was prepared at 0.25 M in water:acetonitrile 1:1 v/v.

4-methylvaleric acid was added as internal standard. Samples were mixed with NPH stock and EDC stock at 1:1:1 ratio by volume. The mixture was heated by heating block at 60°C for 30 min. Samples were filtered through 0.22 μm filters and transferred into HPLC vials and stored at 4°C before analysis.

LC conditions: The instrument used for quantification of butyrate was Agilent 1290 UHPLC. Column: ThermoScientific C18 4.6 × 50 mm, 1.8 μm particle size, at room temperature. Mobile phase A: water with 0.1% v/v formic acid. Mobile phase B: acetonitrile with 0.1% v/v formic acid. Injection volume: 5.0 μL. Flow rate: 0.5 mL/min. Gradient of solvent: 15% mobile phase B at 0.0 min; 100% mobile phase B at 3.5 min; 100% mobile phase B at 6.0 min; 15% mobile phase B at 6.5 min.

ESI-MS/MS method: The instrument used to detect butyrate was an Agilent 6460 Triple Quad MS-MS. Both derivatized butyrate-NPH and 4-methylvaleric-NPH were detected in negative mode. The MS conditions were optimized on pure butyrate-NPH or 4-methylvaleric-NPH at 1 mM. The fragment voltage was 135 V and collision energy was set to 18 V. Multiple reaction monitoring (MRM) of 222 → 137 was assigned to butyrate **(Fig. S13b**), and MRM of 250 → 137 was assigned to 4-methylvaleric acid as internal standard. The ratio between MRM of butyrate and 4-methylvaleric acid was used to quantify the concentration of butyrate.

RNA sequencing and data analysis

Starting at the time of weaning, GF C3H/HeN mice were i.g. administered with PBS, NtL-ButM, or control polymer at 0.8 mg/g of body weight once daily for one week. After that time, mice were euthanized, and the ileum tissue was collected and washed thoroughly. The ileal epithelial cells (IECs) were separated from intestinal tissue by inverting ileal tissue in 0.30 mM EDTA, incubating on ice for 30 min with agitation every 5 min. RNA was extracted from the IECs using an RNA isolation kit (Thermo Fisher Scientific) according to manufacturer's instruction. RNA samples were submitted to the University of Chicago Functional Genomics Core for library preparation and

sequencing on a HiSeq2500 instrument (Illumina, Inc.). 50bp single-end (SE) reads were generated. The quality of raw sequencing reads was assessed by FastQC (v0.11.5). Transcript abundance was quantified by Kallisto (v0.45.0) with Gencode gene annotation (release M18, GRCm38.p6), summarized to gene level by tximport (v1.12.3), Trimmed Mean of M-values (TMM) normalized, and log2 transformed. Lowly expressed genes were removed (defined as, counts per million reads mapped [CPM] <3). Differentially expressed genes (DEGs) between groups of interest were detected using limma voom with precision weights (v3.40.6)[55]. Experimental batch and gender were included as covariates for the model fitting. Significance level and fold changes were computed using empirical Bayes moderated t-statistics test implemented in limma. Significant DEGs were filtered by FDR-adjusted $P<0.05$ and fold change ≥ 1.5 or ≤ −1.5. A more stringent P-value cutoff (e.g., FDR-adjusted $P<0.005$) may be used for visualization of a select number of genes on expression heatmaps.

Intelectin stain and microscope imaging

GF C57BL/6 mice were i.g. administered NtL-ButM at 0.8 mg/g of body weight or PBS once daily for one week beginning at weaning. After that time, the mice were euthanized and perfused, small intestine tissue was obtained, rolled into Swiss-rolls, and prepared into tissue section slides. The tissue section slides were fixed and stained with fluorescent anti-intelectin antibody (R&D Systems, Clone 746420) and DAPI (ProLong antifade reagent with DAPI). The slides were imaged using a Leica fluorescence microscope. Images were processed by ImageJ software and data were plotted and analyzed by Prism software.

In vivo FITC-dextran permeability assay

SPF C57BL/6 8-10 wks old female mice were treated with 2.5% DSS in their drinking water for 7 days. The mice received intragastric administration twice daily, at approximately 10-12 hr intervals, of either PBS, or ButM (800, 400 or 200 mg/kg), or once daily with CsA at 75 mg/kg as

the positive treatment control. On day 7, DSS was removed from the drinking water for the remainder of the study. On day 10, mice were fasted for 3 hr and dosed with 0.1 mL of FITC-dextran 4kDa (at 100 mg/mL). 4 hr post dose mice were anesthetized with isoflurane and bled to exsanguination followed by cervical dislocation. The concentration of FITC in the serum was determined by spectrofluorometry using as standard serially diluted FITC-dextran. Serum from mice not administered FITC-dextran was used to determine the background. A similar permeability assay was also performed in the antibiotic-depletion model as previously described[19]. Littermate-controlled SPF C57BL/6 mice at 2 wks of age were gavaged daily with a mixture of antibiotics (0.4 mg kanamycin sulfate, 0.035 mg gentamycin sulfate, 850U colistin sulfate, 0.215 mg metronidazole, and 0.045 mg vancomycin hydrochloride in 100 µL PBS) for 7 days until weaning. At weaning, mice were then treated with either PBS or ButM (0.8mg/g) twice daily for 7 days. After the final treatment, the mice were fasted for 3 hr. and dosed with 50mg/kg body weight of FITC-dextran 4kDa (at 50 mg/mL). Blood was collected at 1.5 hr. post-administration via cheek bleed and the concentration of FITC in the serum was measured as described above.

Peanut sensitization, ButM treatment and challenge

SPF C3H/HeN mice were treated with 0.45 mg of vancomycin in 0.1 mL by intragastric gavage for 7 days pre-weaning and then with 200 mg/L vancomycin in the drinking water throughout the remainder of the sensitization protocol. Age- and sex-matched 3-wk-old littermates were sensitized weekly by intragastric gavage with defatted, in-house made peanut extract prepared from unsalted roasted peanuts (Hampton Farms, Severn, NC) and cholera toxin (CT) (List Biologicals, Campbell, CA) as previously described[19,39]. Sensitization began at weaning and continued for 4 weeks. Prior to each sensitization the mice were fasted for 4-5 hr and then given 200 µl of 0.2M sodium bicarbonate to neutralize stomach acids. 30 min later the mice received 6 mg of peanut extract and 10 µg of cholera toxin (CT) in 150 µl of PBS by intragastric gavage.

After 4 weeks of sensitization, mice were permitted to rest for 1 wk before a subset of mice was challenged by intraperitoneal (i.p.) administration of 1 mg peanut extract in 200 μl of PBS to confirm that the sensitization protocol induced a uniform allergic response. Rectal temperature was measured immediately following challenge every 10 minutes for up to 90 min using an intrarectal probe, and the change in core body temperature of each mouse was recorded. The remaining mice were not challenged and were randomly assigned into experimental groups. In the monotherapy experiment (**Fig. 5**), one group of mice was treated with ButM twice daily by intragastric gavage at 0.8 mg of total polymer per gram of mouse body weight (0.8 mg/g) for two weeks, and another group of mice received PBS. In the dose-dependent study (**Fig. S17**), mice were treated with either PBS, ButM at 0.8 mg/g (full dose), or ButM at 0.4 mg/g (half dose) twice daily. Additionally, in the experiment where ButM was delivered synchronously with low dose exposure to allergen (**Fig. S18**), one group of mice was treated daily for two weeks with low dose (200 μg) of peanut powder (PB2™ (PB2 Foods, Tifton, GA), and another group of mice received both PB2™ (200 μg) daily and ButM at 0.8 mg/g twice daily. After the treatment window, mice were challenged with i.p. administration of 1 mg peanut extract and core body temperature was measured for 90 min. Serum was collected from mice 90 minutes after challenge for measurement of mMCPT-1 and additionally at 24 hr after challenge for measurement of peanut-specific IgE. Collected blood was incubated at room temperature for 1 hour and centrifuged for 7 minutes at 12,000 g at room temperature, and sera were collected and stored at $^{-}80^{o}C$ before analysis. Serum antibodies and mMCPT-1 were measured by ELISA.

Measurement of mouse mast cell protease 1 (mMCPT-1) and serum peanut-specific IgE antibodies using ELISA

mMCPT-1 was detected using the MCPT-1 mouse uncoated ELISA kit (ThermoFisher) following the protocol provided by manufacturer. For the peanut-specific IgE ELISA, sera from individual mice were added to peanut coated Maxisorp Immunoplates (Nalge Nunc International, Naperville,

IL). Peanut-specific IgE Abs were detected with goat anti-mouse IgE-unlabeled (Southern Biotechnology Associates, Birmingham, AL) and rabbit anti-goat IgG-alkaline phosphatase (Invitrogen, Eugene, Oregon) and developed with p-nitrophenyl phosphate "PNNP" (SeraCare Life Sciences, Inc. Milford, MA). OD values were converted to nanograms per milliliter of IgE by comparison with standard curves of purified IgE by linear regression analysis and are expressed as the mean concentration for each group of mice ± s.e.m. Statistical differences in serum Ab levels were determined using a two-tailed Student's t test. A P value < 0.05 was considered significant.

16S rRNA targeted sequencing

Bacterial DNA was extracted using the QIAamp PowerFecal Pro DNA kit (Qiagen). The V4-V5 hypervariable region of the 16S rRNA gene from the purified DNA was amplified using universal bacterial primers – 563F (5'-nnnnnnnn-NNNNNNNNNNNN-AYTGGGYDTAAA-GNG-3') and 926R (5'-nnnnnnnn-NNNNNNNNNNNN-CCGTCAATTYHT- TTRAGT-3'), where 'N' represents the barcodes, 'n' are additional nucleotides added to offset primer sequencing. Illumina sequencing-compatible Unique Dual Index (UDI) adapters were ligated onto pools using the QIAsep 1-step amplicon library kit (Qiagen). Library QC was performed using Qubit and Tapestation before sequencing on an Illumina MiSeq platform at the Duchossois Family Institute Microbiome Metagenomics Facility at the University of Chicago. This platform generates forward and reverse reads of 250 bp which were analyzed for amplicon sequence variants (ASVs) using the Divisive Amplicon Denoising Algorithm (DADA2 v1.14)[56]. Taxonomy was assigned to the resulting ASVs using the Ribosomal Database Project (RDP) database with a minimum bootstrap score of 50[57]. The ASV tables, taxonomic classification, and sample metadata were compiled using the phyloseq data structure[58]. Subsequent 16S rRNA relative abundance analyses and visualizations were performed using R version 4.1.1 (R Development Core Team, Vienna, Austria).

Microbiome analysis

To identify changes in the microbiome across conditions, a linear discriminant analysis effect size (LEfSe) analysis was performed in R using the microbiomeMarker package and the run_lefse function[59,60]. Features, specifically taxa, can be associated with or without a given condition (e.g., ButM post-treatment vs PBS post-treatment) and an effect size can be ascribed to that difference in taxa at a selected taxonomic level (LDA score). For the LEfSe analysis, genera were compared as the main group, a significance level of 0.05 was chosen for both the Kruskall-Wallis and Wilcoxon tests and a linear discriminant analysis cutoff of 1.0 was implemented. The abundance of *Clostridium* Cluster XIVA in post-treatment samples was also determined by quantitative PCR (qPCR) using the same DNA analyzed by 16S rRNA targeted sequencing. Commonly used primers 8F[61] and 338R[62] were used to quantify total copies of the 16S rRNA gene for normalization purposes. Primers specific for *Clostridium* Cluster XIVa[63] were validated by PCR and qPCR. Primer sequences are listed in **Supplementary Table S1**. qPCR was performed using PowerUp SYBR green master mix (Applied Bioystems) according to manufacturer's instructions. The abundance of *Clostridium* Cluster XIVa is calculated by 2^{-CT}, multiplied by a constant to bring all values above 1 (1×10^{16}), and expressed as a ratio to total copies 16S per gram of raw fecal content.

Toxicity study

The toxicity effect of pHPMA-b-pBMA on SPF C3H/HeJ mice was measured by hematological analysis on Vet Axcel Chemistry Analyzer. Mice were treated with NtL-ButM at 0.8 mg/g of body weight daily by intragastric gavage for 6 weeks. Every week, a blood sample of each mouse was obtained and analyzed by the chemistry analyzer according to manufacturer's instruction.

Statistical analysis

Statistical analysis and plotting of data were performed using Prism 9.0 (Graphpad), as indicated in the figure legends. One-way ANOVA with Dunnett's post-test for multiple comparisons were used in **Fig. 4b**. Two-sided Student's t-test was used in **Fig. 3c** and **Fig. 5e-f**. In **Fig. 5d**, the area under curve (AUC) values of temperature changes were compared using two-sided Student's t-test. Data represent mean ± s.e.m.; *n* is stated in the figure legend.

Code availability

Custom codes and scripts on the RNA sequencing analysis, genomic analysis, and microbiome analysis are available from the corresponding author upon request.

Data availability

The main data supporting the results in this study are available within the paper and its Supplementary Information. Additional processed data are available from the corresponding authors upon request.

Acknowledgements

This work was supported by a sponsored research agreement from ClostraBio, Inc., and partially supported by the Chicago Immunoengineering Innovation Center of the University of Chicago. D.S.W. was supported by a fellowship from the Whitaker Foundation. We thank Matthew Bauer and Suzana Gomes for technical assistance. We thank Dr. Betty Theriault from GRAF and Pieter Faber from the Genomics Facility. Parts of this work were carried out at the Cytometry and Antibody Technology Core Facility (Cancer Center Support Grant P30CA014599), the Duchossois Family Institute Microbiome Metagenomics Facility, the Soft Matter Characterization Facility, the Mass Spectrometry Facility (NSF instrumentation grant CHE-1048528), the Nuclear Magnetic Resonance Facility, the Advanced Electron Microscopy Facility (RRID:SCR_019198), and the Functional Genomics Core at the University of Chicago, and the SLAC National

Accelerator Laboratory. Some of the bioinformatics analysis was performed on the high-performance computing (HPC) clusters at the University of Chicago Center for Research Informatics, and we thank M. Jarsulic for his technical assistance on the HPC clusters.

Author contributions

C.R.N. and J.A.H. oversaw all research. R.W., S.C., M.E.H.B., C.R.N., and J.A.H. designed the research strategy. R.W., D.S.W, and J.A.H. conceptualized materials. R.W. and S.C. synthesized materials and fabricated micelles. R.W., S.C., M.E.H.B, L.A.H., Y.S., S.M.C.H., A.T., E.C. M.S., H.N.S, and H.W. performed experiments. R.W., S.C., M.E.H.B, and L.A.H. analyzed experiments. R.B. performed data analysis on the RNA sequencing experiment, N.P.D. and E.C. performed 16S rRNA targeted microbiome analysis. R.W., S.C., C.R.N, and J.A.H. wrote the manuscript. All authors contributed to the article and approved the submitted version.

Competing interests

C.R.N. and J.A.H. are founders and shareholders in ClostraBio, Inc, which is developing the technology described herein. R.W., S.C., M.E.H.B., D.S.W., C.R.N. and J.A.H. are inventors on patents filed by the University of Chicago describing the micelles reported herein.

References

1. Iweala, O.I. & Nagler, C.R. The Microbiome and Food Allergy. *Annual Review of Immunology* **37**, 377-403 (2019).
2. Bao, R.*, et al.* Fecal microbiome and metabolome differ in healthy and food-allergic twins. *J Clin Invest* **131**(2021).
3. Feehley, T.*, et al.* Healthy infants harbor intestinal bacteria that protect against food allergy. *Nature Medicine* (2019).
4. Kim, C.H. Control of lymphocyte functions by gut microbiota-derived short-chain fatty acids. *Cell Mol Immunol* **18**, 1161-1171 (2021).
5. Tan, J.*, et al.* The role of short-chain fatty acids in health and disease. *Adv Immunol* **121**, 91-119 (2014).
6. Zheng, L.*, et al.* Microbial-Derived Butyrate Promotes Epithelial Barrier Function through IL-10 Receptor-Dependent Repression of Claudin-2. *J Immunol* **199**, 2976-2984 (2017).
7. Gupta, R.S.*, et al.* Prevalence and Severity of Food Allergies Among US Adults. *JAMA Netw Open* **2**, e185630-e185630 (2019).
8. Chinthrajah, R.S.*, et al.* Sustained outcomes in oral immunotherapy for peanut allergy (POISED study): a large, randomised, double-blind, placebo-controlled, phase 2 study. *The Lancet* **394**, 1437-1449 (2019).
9. Honda, K. & Littman, D.R. The microbiota in adaptive immune homeostasis and disease. *Nature* **535**, 75-84 (2016).
10. Belkaid, Y. & Harrison, O.J. Homeostatic Immunity and the Microbiota. *Immunity* **46**, 562-576 (2017).
11. Wells, J.M.*, et al.* Homeostasis of the gut barrier and potential biomarkers. *Am J Physiol Gastrointest Liver Physiol* **312**, G171-g193 (2017).
12. Donohoe, D.R.*, et al.* The microbiome and butyrate regulate energy metabolism and autophagy in the mammalian colon. *Cell metabolism* **13**, 517-526 (2011).
13. Koh, A., De Vadder, F., Kovatcheva-Datchary, P. & Bäckhed, F. From Dietary Fiber to Host Physiology: Short-Chain Fatty Acids as Key Bacterial Metabolites. *Cell* **165**, 1332-1345 (2016).
14. Kelly, C.J.*, et al.* Crosstalk between Microbiota-Derived Short-Chain Fatty Acids and Intestinal Epithelial HIF Augments Tissue Barrier Function. *Cell Host Microbe* **17**, 662-671 (2015).
15. Bevins, C.L. & Salzman, N.H. Paneth cells, antimicrobial peptides and maintenance of intestinal homeostasis. *Nature Reviews Microbiology* **9**, 356-368 (2011).
16. Arpaia, N.*, et al.* Metabolites produced by commensal bacteria promote peripheral regulatory T-cell generation. *Nature* **504**, 451-455 (2013).
17. Furusawa, Y.*, et al.* Commensal microbe-derived butyrate induces the differentiation of colonic regulatory T cells. *Nature* **504**, 446 (2013).
18. Smith, P.M.*, et al.* The microbial metabolites, short-chain fatty acids, regulate colonic Treg cell homeostasis. *Science* **341**, 569-573 (2013).
19. Stefka, A.T.*, et al.* Commensal bacteria protect against food allergen sensitization. *Proc Natl Acad Sci U S A* **111**, 13145-13150 (2014).
20. Nagler, C.R. Drugging the microbiome. *J Exp Med* **217**, e20191642 (2020).
21. Jimenez, M., Langer, R. & Traverso, G. Microbial therapeutics: New opportunities for drug delivery. *J Exp Med* **216**, 1005-1009 (2019).
22. Liu, H.*, et al.* Butyrate: A Double-Edged Sword for Health? *Adv Nutr* **9**, 21-29 (2018).
23. Tan, J.*, et al.* Dietary Fiber and Bacterial SCFA Enhance Oral Tolerance and Protect against Food Allergy through Diverse Cellular Pathways. *Cell Reports* **15**, 2809-2824 (2016).
24. Cait, A.*, et al.* Microbiome-driven allergic lung inflammation is ameliorated by short-chain fatty acids. *Mucosal Immunology* **11**, 785 (2017).

25. Sun, M.*, et al.* Microbiota-derived short-chain fatty acids promote Th1 cell IL-10 production to maintain intestinal homeostasis. *Nature Communications* **9**, 3555 (2018).
26. Xu, F., Xu, J.W. & Luo, Y.L. Impact of hydrogenation on physicochemical and biomedical properties of pH-sensitive PMAA-b-HTPB-b-PMAA triblock copolymer drug carriers. *J Biomater Appl* **30**, 1473-1484 (2016).
27. Colombani, O.*, et al.* Synthesis of Poly(n-butyl acrylate)-block-poly(acrylic acid) Diblock Copolymers by ATRP and Their Micellization in Water. *Macromolecules* **40**, 4338-4350 (2007).
28. Colombani, O.*, et al.* Structure of Micelles of Poly(n-butyl acrylate)-block-poly(acrylic acid) Diblock Copolymers in Aqueous Solution. *Macromolecules* **40**, 4351-4362 (2007).
29. Felber, A.E., Dufresne, M.-H. & Leroux, J.-C. pH-sensitive vesicles, polymeric micelles, and nanospheres prepared with polycarboxylates. *Advanced Drug Delivery Reviews* **64**, 979-992 (2012).
30. Aguiar, J., Carpena, P., Molina-Bolívar, J.A. & Carnero Ruiz, C. On the determination of the critical micelle concentration by the pyrene 1:3 ratio method. *Journal of Colloid and Interface Science* **258**, 116-122 (2003).
31. Wu, H., Ting, J.M., Weiss, T.M. & Tirrell, M.V. Interparticle Interactions in Dilute Solutions of Polyelectrolyte Complex Micelles. *ACS Macro Letters* **8**, 819-825 (2019).
32. Torii, T.*, et al.* Measurement of short-chain fatty acids in human faeces using high-performance liquid chromatography: specimen stability. *Ann Clin Biochem* **47**, 447-452 (2010).
33. Tyagi, A.M.*, et al.* The Microbial Metabolite Butyrate Stimulates Bone Formation via T Regulatory Cell-Mediated Regulation of WNT10B Expression. *Immunity* **49**, 1116-1131.e1117 (2018).
34. Lele, B.S. & Hoffman, A.S. Mucoadhesive drug carriers based on complexes of poly(acrylic acid) and PEGylated drugs having hydrolysable PEG-anhydride-drug linkages. *J Control Release* **69**, 237-248 (2000).
35. Serra, L., Doménech, J. & Peppas, N.A. Engineering design and molecular dynamics of mucoadhesive drug delivery systems as targeting agents. *European Journal of Pharmaceutics and Biopharmaceutics* **71**, 519-528 (2009).
36. Tsuji, S.*, et al.* Human intelectin is a novel soluble lectin that recognizes galactofuranose in carbohydrate chains of bacterial cell wall. *J Biol Chem* **276**, 23456-23463 (2001).
37. Castillo, P.A.*, et al.* An Experimental Approach to Rigorously Assess Paneth Cell α-Defensin (Defa) mRNA Expression in C57BL/6 Mice. *Scientific Reports* **9**, 13115 (2019).
38. Cochran, K.E., Lamson, N.G. & Whitehead, K.A. Expanding the utility of the dextran sulfate sodium (DSS) mouse model to induce a clinically relevant loss of intestinal barrier function. *PeerJ* **8**, e8681-e8681 (2020).
39. Bashir, M.E.H., Louie, S., Shi, H.N. & Nagler-Anderson, C. Toll-Like Receptor 4 Signaling by Intestinal Microbes Influences Susceptibility to Food Allergy. *The Journal of Immunology* **172**, 6978 (2004).
40. Sorobetea, D., Holm, J.B., Henningsson, H., Kristiansen, K. & Svensson-Frej, M. Acute infection with the intestinal parasite Trichuris muris has long-term consequences on mucosal mast cell homeostasis and epithelial integrity. *Eur J Immunol* **47**, 257-268 (2017).
41. Bramhall, M. & Zaph, C. Mastering gut permeability: New roles for old friends. *Eur J Immunol* **47**, 236-239 (2017).
42. PALISADE Group of Clinical Investigators. AR101 oral immunotherapy for peanut allergy. *New England Journal of Medicine* **379**, 1991-2001 (2018).
43. Atarashi, K.*, et al.* Induction of colonic regulatory T cells by indigenous Clostridium species. *Science* **331**, 337-341 (2011).

44. Lopetuso, L.R., Scaldaferri, F., Petito, V. & Gasbarrini, A. Commensal Clostridia: leading players in the maintenance of gut homeostasis. *Gut Pathogens* **5**, 23 (2013).
45. Byndloss, M.X.*, et al.* Microbiota-activated PPAR-γ signaling inhibits dysbiotic Enterobacteriaceae expansion. *Science* **357**, 570-575 (2017).
46. Gupta, R.S.*, et al.* The Public Health Impact of Parent-Reported Childhood Food Allergies in the United States. *Pediatrics* **142**, e20181235 (2018).
47. Rossen, N.G.*, et al.* Findings From a Randomized Controlled Trial of Fecal Transplantation for Patients With Ulcerative Colitis. *Gastroenterology* **149**, 110-118.e114 (2015).
48. Nair, A.B. & Jacob, S. A simple practice guide for dose conversion between animals and human. *J Basic Clin Pharm* **7**, 27-31 (2016).
49. Vernero, M.*, et al.* The Usefulness of Microencapsulated Sodium Butyrate Add-On Therapy in Maintaining Remission in Patients with Ulcerative Colitis: A Prospective Observational Study. *Journal of clinical medicine* **9**, 3941 (2020).
50. Luceri, C.*, et al.* Effect of butyrate enemas on gene expression profiles and endoscopic/histopathological scores of diverted colorectal mucosa: A randomized trial. *Digestive and Liver Disease* **48**, 27-33 (2016).
51. Facchin, S.*, et al.* Microbiota changes induced by microencapsulated sodium butyrate in patients with inflammatory bowel disease. *Neurogastroenterology & Motility* **32**, e13914 (2020).
52. Cai, R., Li, R., Qian, J., Xie, A. & Nie, K. The morphology and fabrication of nanostructured micelle by a novel block copolymer with linear–dendritic structure. *Materials Science and Engineering: C* **33**, 2070-2077 (2013).
53. Megías, C.*, et al.* Stability of sunflower protein hydrolysates in simulated gastric and intestinal fluids and Caco-2 cell extracts. *LWT - Food Science and Technology* **42**, 1496-1500 (2009).
54. Fu, T.J., Abbott, U.R. & Hatzos, C. Digestibility of food allergens and nonallergenic proteins in simulated gastric fluid and simulated intestinal fluid-a comparative study. *J Agric Food Chem* **50**, 7154-7160 (2002).
55. Law, C.W., Chen, Y., Shi, W. & Smyth, G.K. voom: precision weights unlock linear model analysis tools for RNA-seq read counts. *Genome Biology* **15**, R29 (2014).
56. Callahan, B.J.*, et al.* DADA2: High-resolution sample inference from Illumina amplicon data. *Nature Methods* **13**, 581-583 (2016).
57. Wang, Q., Garrity George, M., Tiedje James, M. & Cole James, R. Naïve Bayesian Classifier for Rapid Assignment of rRNA Sequences into the New Bacterial Taxonomy. *Applied and Environmental Microbiology* **73**, 5261-5267 (2007).
58. McMurdie, P.J. & Holmes, S. phyloseq: An R Package for Reproducible Interactive Analysis and Graphics of Microbiome Census Data. *PLOS ONE* **8**, e61217 (2013).
59. Segata, N.*, et al.* Metagenomic biomarker discovery and explanation. *Genome Biology* **12**, R60 (2011).
60. Yang, C. Microbiome R package: microbiome biomarker analysis toolkit. R package version 0.99.0. (2020).
61. Turner, S., Pryer, K.M., Miao, V.P.W. & Palmer, J.D. Investigating Deep Phylogenetic Relationships among Cyanobacteria and Plastids by Small Subunit rRNA Sequence Analysis1. *Journal of Eukaryotic Microbiology* **46**, 327-338 (1999).
62. Amann, R.I., Ludwig, W. & Schleifer, K.H. Phylogenetic identification and in situ detection of individual microbial cells without cultivation. *Microbiological Reviews* **59**, 143-169 (1995).
63. Matsuki, T.*, et al.* Development of 16S rRNA-gene-targeted group-specific primers for the detection and identification of predominant bacteria in human feces. *Applied and environmental microbiology* **68**, 5445-5451 (2002).

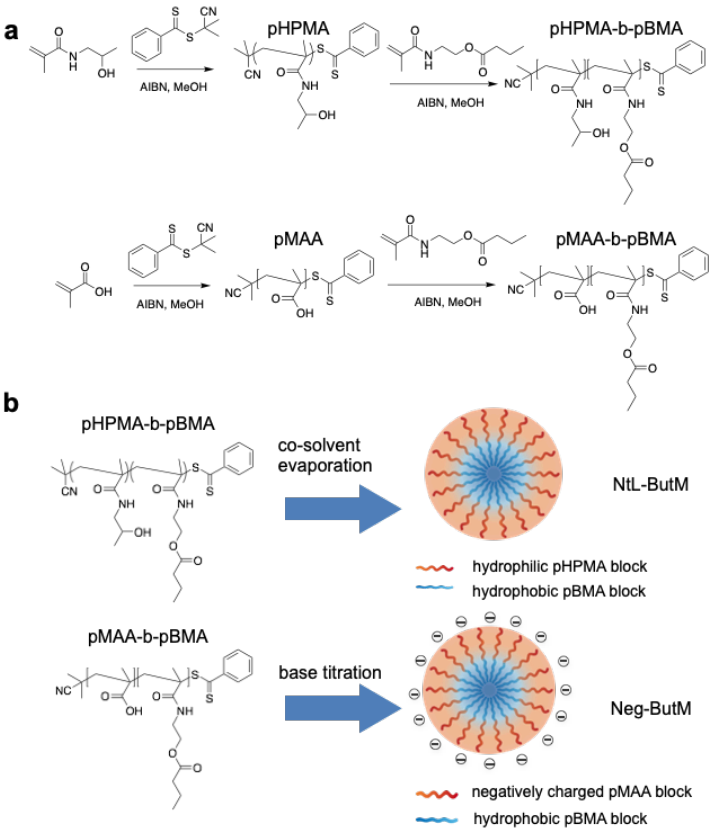

e

	Size (nm, diameter)	ζ-potential (mV)	CMC (μM)	Radius of gyration (nm)	Aggregation number
NtL-ButM	44.7 ± 0.8	-0.34 ± 0.5	0.8 ± 0.4	14.2	119
Neg-ButM	39.9 ± 1.6	-31.5 ± 2.3	14.0 ± 3.5	13.5	92

Fig. 1. Chemical composition and structural characterization of butyrate-prodrug micelles, namely NtL-ButM, consisting of the neutral block copolymer pHPMA-b-pBMA, and Neg-ButM, consisting of the anionic block copolymer pMAA-b-pBMA. **a,** Synthetic route of pHPMA-b-pBMA and pMAA-b-pBMA. **b,** (**upper**) The NtL-ButM contains a hydrophilic (HPMA) block as the micelle corona, while a hydrophobic (BMA) block forms the micelle core. (**lower**) The Neg-ButM contains a hydrophilic (MAA) block that forms a negatively charged micelle corona, and the same hydrophobic (BMA) block as NtL-ButM. **c**, **d,** Cryogenic electron microscopy (CryoEM) images show the spherical structures of micelles NtL-ButM (**c**) or Neg-ButM (**d**). **e,** Table summarizing the characterization of micelles NtL-ButM and Neg-ButM, including hydrodynamic diameter and zeta-potential from DLS, critical micelle concentration, radius of gyration and aggregation number from SAXS.

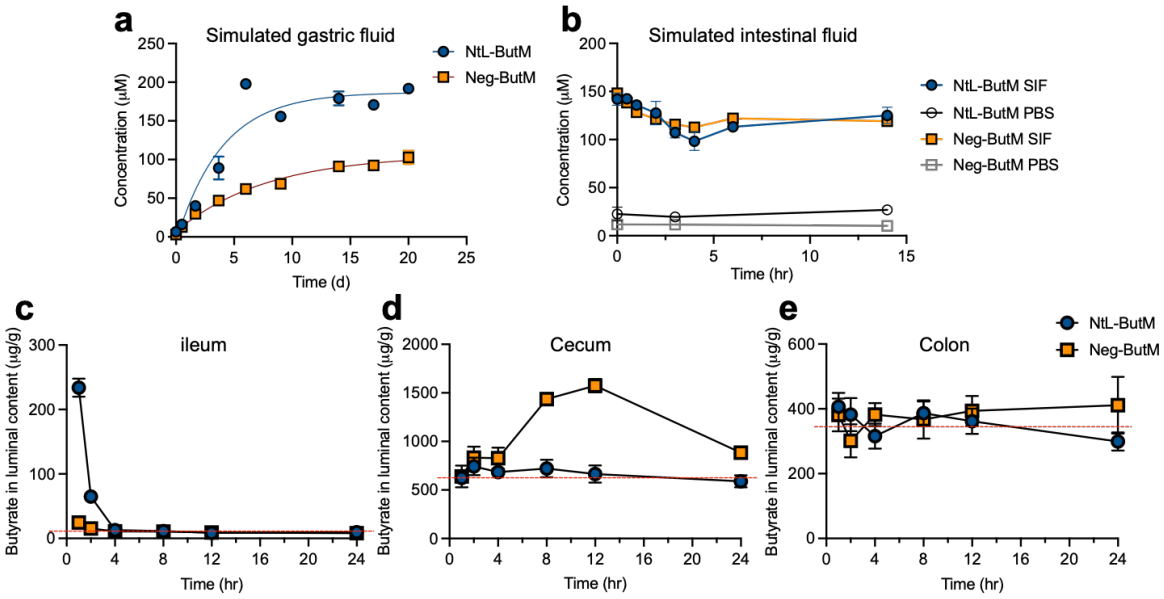

Fig. 2. *In vitro* and *in vivo* butyrate release in the GI tract from NtL-ButM and Neg-ButM. **a,** Both NtL-ButM and Neg-ButM released butyrate slowly in the simulated gastric fluid over 20 days. **b,** Both NtL-ButM and Neg-ButM released their complete butyrate load within minutes in simulated intestinal fluid (SIF) containing high levels of the esterase pancreatin. Neither polymer released butyrate in PBS on these timescales. n = 3. **c-e**, The amount of butyrate released in the ileum, cecum, or colon contents after a single intragastric administration of NtL-ButM or Neg-ButM at 0.8 mg/g to SPF C3H/HeJ mice. Butyrate was derivatized with 3-nitrophenylhydrazine and quantified with LC-MS/MS (ileum samples) or LC-UV (cecum and colon samples). The dotted red lines represent butyrate content in untreated mice. n = 9-10 mice per group. Data represent mean ± s.e.m.

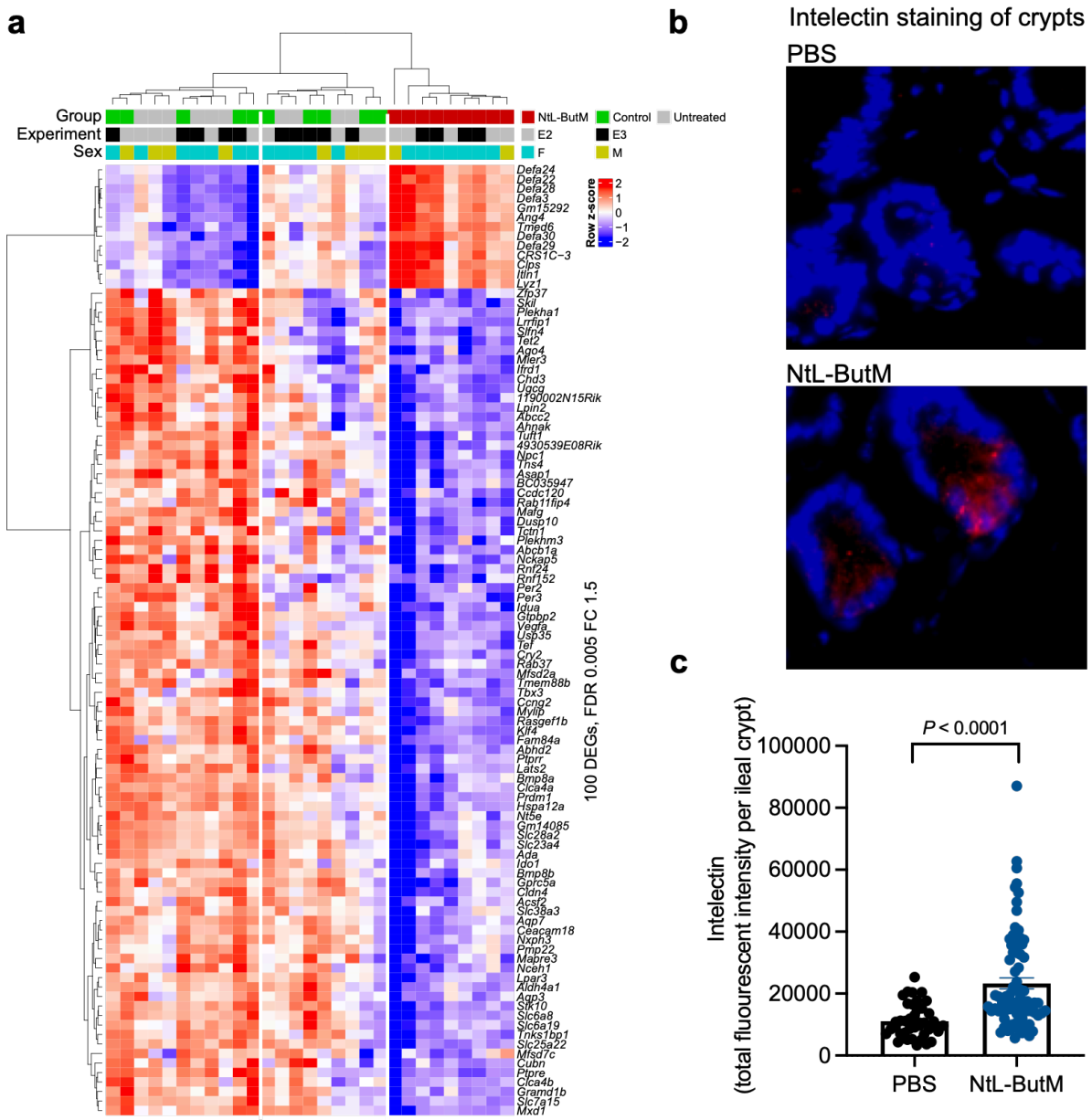

Fig. 3. NtL-ButM induced an ileal gene expression signature that is almost entirely anti-microbial peptides (AMPs). a, One week of daily dosing of 0.8 mg/g NtL-ButM to germ-free (GF) C3H/HeN mice induces a unique gene expression signature in the ileum compared to untreated and inactive polymer controls as measured by RNA sequencing of isolated intestinal epithelial cells. Top 100 significant differentially expressed genes (DEGs) at False Discovery Rate (FDR)-adjusted P<0.005 and fold change (FC) ≥ 1.5 or ≤−1.5 are shown. Annotation bars of the three groups, experiment batches (E2 and E3), and gender (female, male) are shown above the heatmap. **b,** Fluorescent imaging of intelectin protein in small intestine sections from control or treated mice. Blue (DAPI), red (intelectin). **c,** Intelectin protein is quantified by total fluorescence signal per crypt of small intestine. n = 3 PBS-treated and 4 NtL-ButM treated mice, with >15 crypts quantified per mouse. Data represent mean ± s.e.m. limma voom with precision weights was used in **a**. Two-sided Student's t-test was used in **c**.

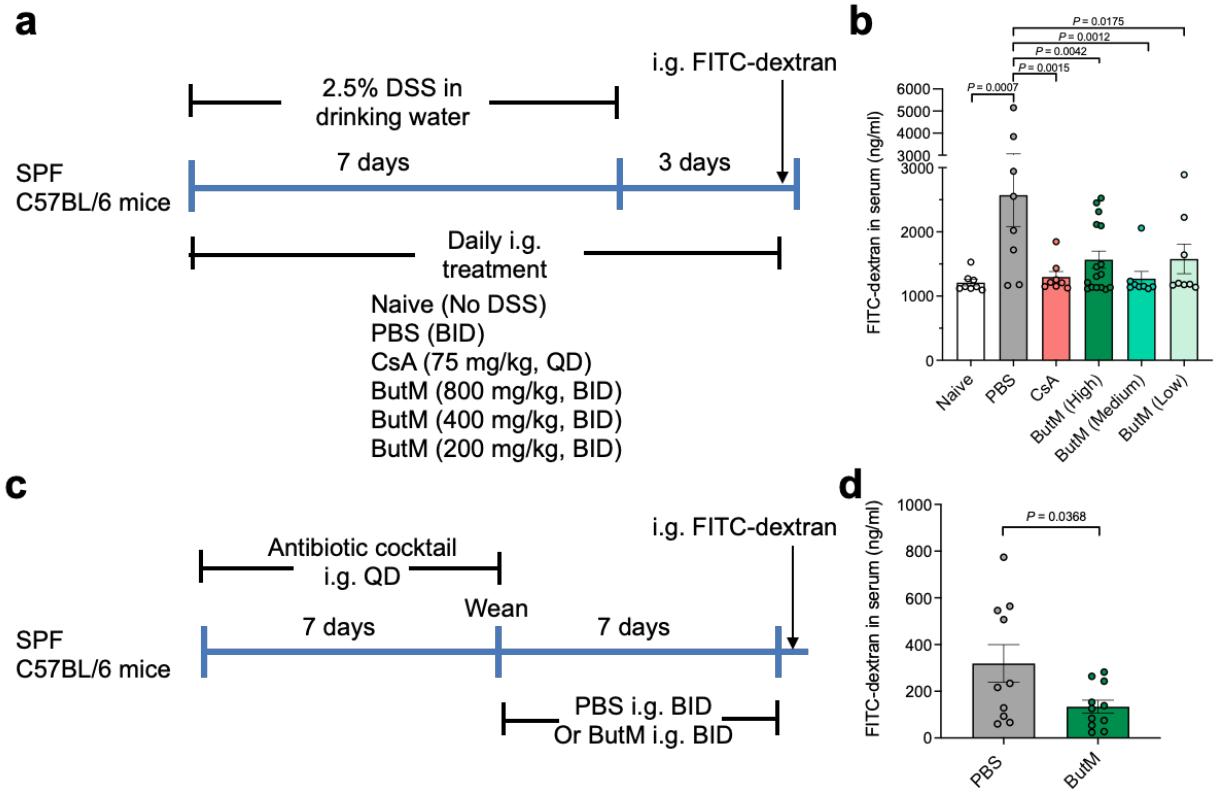

Fig. 4. Butyrate micelle treatment repaired intestinal barrier integrity in DSS-treated or antibiotic-treated mice. **a,** Mice were given 2.5% DSS in the drinking water for 7 days to induce epithelial barrier dysfunction. DSS was removed from the drinking water on days 7-10. For treatment mice were intragastrically (i.g.) dosed daily with either PBS, cyclosporin A (CsA), or ButM at different concentrations. QD: once a day, BID: twice daily at 10-12 hr intervals. On day 10, all mice received an i.g. administration of 4kDa FITC-dextran. Fluorescence was measured in the serum 4 hr later. **b,** Concentration of FITC-dextran in the serum. n=8 mice per group, except for high dose ButM which had 16 mice per group. **c**, Mice were treated with a mixture of antibiotics, beginning at 2 wk of age, for 7 days. After weaning, mice were i.g. administered either PBS (n=10) or ButM (n=11) at 800 mg/kg twice daily for 7 days. All mice then received an i.g. administration of 4kDa FITC-dextran. Fluorescence was measured in the serum 1.5 hr later. **d**, Concentration of FITC-dextran in the serum. Data in **d** is pooled from two independent experiments. Data represent mean ± s.e.m. Comparisons were made using one-way ANOVA with Dunnett's post-test (**c**), or Student's t-test (**d**).

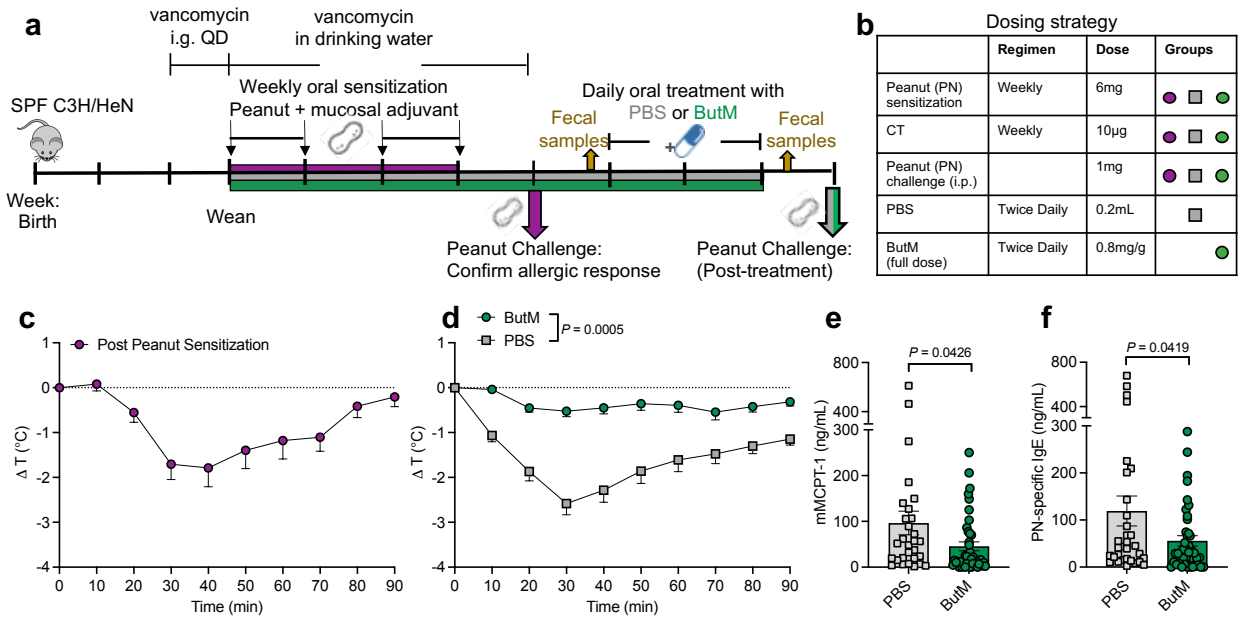

Fig. 5. Butyrate micelle treatment reduced the anaphylactic response to peanut challenge. a, b, Experimental schema and dosing strategy. All of the mice were sensitized weekly by intragastric gavage of 6 mg of peanut extract (PN) plus 10 µg of the mucosal adjuvant cholera toxin. After 4 weeks of sensitization one group of mice (n=20) was challenged by i.p. administration of 1 mg of PN to confirm that the sensitization protocol induced a uniform allergic response. Fecal samples were collected before and after treatment for microbiome analysis in **Fig. 6.** (**c**). Change in core body temperature following PN challenge where core body temperature drop indicates anaphylaxis. The remaining mice were randomized into two treatment groups. One group was treated with PBS (n=32) and the other group was treated with a 1:1 mix of NtL-ButM and Neg-ButM polymers 0.4 mg/g each (n=41). QD: once a day, BID: twice daily at 10-12 hr intervals. **d,** Change in core body temperature following challenge with PN in PBS or ButM treated mice. The area under curve (AUC) values were compared between two groups. **e,f,** Serum mMCPT-1 (**e**) and peanut-specific IgE (**f**) from mice in **d**. Data represent mean ± s.e.m. Data in **c**, **d** and e is pooled from two independent experiments. Data analyzed using two-sided Student's t-test.

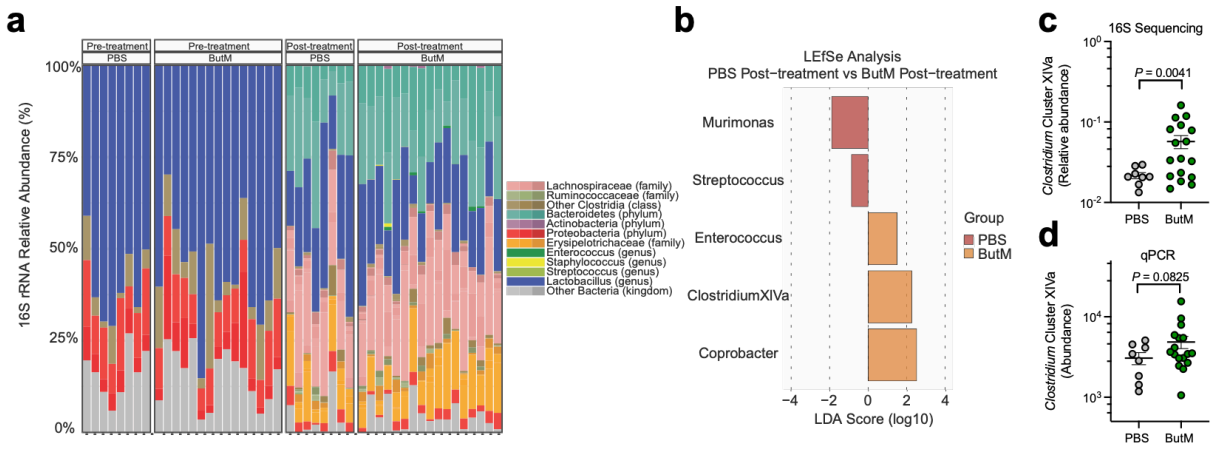

Fig. 6. Butyrate micelles alter the fecal microbiome and promote recovery of *Clostridium* Cluster XIVa after antibiotic exposure. **a**, 16S rRNA sequencing analysis of relative abundance of bacterial taxa in fecal samples of allergic mice collected before (left) or after (right) treatment with PBS (n = 8) or ButM (n = 17) (see **Fig. 5a**). **b**, Differentially abundant taxa between mice treated with PBS or ButM after treatment as analyzed by LEfSe **c,** Relative abundance of *Clostridium* Cluster XIVa in fecal samples after treatment with PBS or ButM (from **a**) or **d,** analyzed by qPCR**.** For **c** and **d**, Student's t-test with Welch's correction was used for statistical analysis.